frontiers in Earth Science

ORIGINAL RESEARCH
published: 11 October 2021
doi: 10.3389/feart.2021.766011

Investigation on Coal Skeleton Deformation in CO_2 Injection Enhanced CH_4 Drainage From Underground Coal Seam

Chaojun Fan[1,2], Lei Yang[1], Gang Wang[2]*, Qiming Huang[2], Xiang Fu[1] and Haiou Wen[1]*

[1]College of Mining, Liaoning Technical University, Fuxin, China, [2]Key Laboratory of Mining Disaster Prevention and Control, Shandong University of Science and Technology, Qingdao, China

OPEN ACCESS

Edited by:
Jienan Pan,
Henan Polytechnic University, China

Reviewed by:
Ting Liu,
China University of Mining and Technology, China
Jun Liu,
Sichuan University, China

***Correspondence:**
Chaojun Fan
chaojunfan@139.com
Gang Wang
gang.wang@sdust.edu.cn

Specialty section:
This article was submitted to Economic Geology, a section of the journal Frontiers in Earth Science

Received: *28 August 2021*
Accepted: *15 September 2021*
Published: *11 October 2021*

Citation:
Fan C, Yang L, Wang G, Huang Q, Fu X and Wen H (2021) Investigation on Coal Skeleton Deformation in CO_2 Injection Enhanced CH_4 Drainage From Underground Coal Seam. Front. Earth Sci. 9:766011. doi: 10.3389/feart.2021.766011

To reveal the evolution law of coal skeleton deformation during the process of CO_2 flooding and displacing CH_4 in coal seam, a fluid-solid coupling mathematical model of CO_2 injection enhanced CH_4 drainage was established based on Fick's law, Darcy's law, ideal gas state equation, and Langmuir equation. Meanwhile, numerical simulations were carried out by implementing the mathematical model in the COMSOL Multiphysics. Results show that the CH_4 content of both regular gas drainage and CO_2 enhanced gas drainage gradually decreases with time, and the decreasing rate is high between 10 and 60 days. Compared with regular gas drainage, the efficiency of CO_2 enhanced gas drainage is more obvious with greater amount of CH_4 extracted out. When coal seam gas is extracted for 10, 60, 120, and 180 days, CH_4 content in coal seam is reduced by 5.2, 17.2, 23.6, and 26.7%, respectively. For regular gas drainage, the deformation of coal skeleton is dominated by the shrink of coal matrix induced by gas desorption, and the strain curve shows a continuous downward trend. For CO_2 enhanced gas drainage, the strain curve of coal skeleton showed a decrease—rapid increase—slow increase trend. The evolution of permeability is opposite to the evolution of coal skeleton strain. Higher gas injection pressure will lead to a greater coal skeleton strain. The pumping pressure affects the deformation of coal skeleton slightly compared with that of initial water saturation and initial temperature. Greater initial water saturation leads to larger deformation of coal skeleton in the early stage. The strain value of coal skeleton gradually tends to be consistent as gas injection prolongs. Higher initial temperature leads to greater reduction in coal skeleton strain when the gas injection continues. Research achievements provide a basis for the field application of CO_2 injection enhanced CH_4 drainage in underground coal mines.

Keywords: coal seam, CO_2 injection enhanced CH_4 drainage, coal skeleton deformation, numerical simulation, fluid-solid coupling model

1 INTRODUCTION

Coal seam gas is a by-product of coal mining, mainly composed of CH_4 (Fan et al., 2017). Coal seam gas is a clean energy source. However, coal and gas outbursts and gas explosions often occur with coal mining, which severely restricts the safe and efficient production of coal mines (Huo et al., 2019). With the increase of mining depth, the permeability of coal seam gradually decreases, resulting in the increase of difficulty of gas drainage. Therefore, improving the efficiency of coal seam gas drainage is a key technology for preventing and controlling mine gas disasters, as well as the development and utilization of gas resources (Guo et al., 2020).

Scholars have explored the method of replacing CH_4 by injecting waste gas into the coal seam. Generally, the injected gas includes CO_2, N_2, and flue gas (Wu et al., 2019). The adsorption capacity of coal for CO_2, N_2, and CH_4 is $CO_2 > CH_4 > N_2$ through a series of studies, which provides a certain theoretical basis for coal seam gas injection (Song et al., 2019, Fan et al., 2019a, Yi et al., 2013). N_2 mainly displaces coal bed methane by changing the pressure gradient in the coal-rock fractures (Lin et al., 2018), and the competitive adsorption effect is small. CO_2 can not only displace the free CH_4 in fractures, but also compete with the gas on the adsorption site to replace it (Liu et al., 2017; Fang et al., 2019a). Busch et al. (2003) carried out CO_2 and CH_4 mixed binary gas adsorption and desorption experiments on different coal ranks under the same conditions, and found that the adsorption capacity of CO_2 is stronger than that of CH_4 (Liu et al., 2019; Wang et al., 2018). Reznik et al. (1984) conducted experiments by injecting CO_2 into bituminous coal containing CH_4 and bituminous coal containing water under high pressure, and proved that CO_2 injection can increase the recovery rate of CH_4 by 2–3 times and obtained higher gas injection pressure can lead to higher recovery rate of CH_4 (Chattaraj et al., 2016, Lin et al., 2017). Baran et al. (2014) used the volumetric method to conduct adsorption experiments under lower and higher pressures, and proved that CO_2 is the best gas that can penetrate into the internal structure of coal. The above experiments show that CO_2 injection can flood or displace coal seam CH_4 and improve the efficiency of CH_4 drainage. To explore the mechanism of CO_2 injection enhanced CH_4 recovery, scholars from various countries have carried out numerical simulation on the basis of physical experiments. Vishal et al. (2015) studied the effect of adsorption time on CO_2 enhanced coal bed methane recovery (CO_2-ECBM). Zhou et al. (2012) and Fang et al. (2019b) used COMSOL Multiphysics software to analyze the evolution of permeability in the CO_2-ECBM process, and the results show that the effective stress changes, matrix shrinkage, and swelling caused by pumping pressure of drainage and CO_2 injection pressure are the key factors affecting permeability. Gas injection pressure and temperature are the two key factors that affect the efficiency of CH_4 extraction (Fang et al., 2019c). Fan et al. (2018) considered non-isothermal adsorption and analyzed the effects of different injection pressures and initial temperatures on CO_2-ECBM. Additionally, Pan et al. (2019) studied the evolution of its microstructural changes under high-pressure methane adsorption/desorption. Wang et al. (2020) revealed the specific process of coal macromolecular rearrangement caused by CO_2 injection through molecular dynamics.

However, predecessors have seldom studied the deformation law of coal skeleton in the process of gas injection to displace coal seam CH_4. In this article the coal mass is considered a dual pore structure composed of pores and fractures, and a fluid-solid coupling model for gas injection enhanced methane drainage is established. The COMSOL Multiphysics software is used to study the coal skeleton strain law in the process of CO_2 injection to displace coal seam CH_4 on the background of Zhangcun coal mine in Shanxi Provence. The results will provide a reference for improving the CH_4 drainage from coal seams during underground mining.

2 MATHEMATICAL MODEL OF CO_2 INJECTION ENHANCED CH_4 DRAINAGE IN COAL SEAM

2.1 Basic Assumptions

According to the occurrence characteristics of gas in coal reservoirs, the following assumptions are made (Fan et al., 2016; Li et al., 2016; Ren et al., 2017; Fan et al., 2019b): 1) The coal mass is a porous medium with double pores composed of pores and fracture; 2) The gas migration in the matrix satisfies Fick's law of diffusion, and the gas migration process in the fracture satisfies Darcy's law; 3) CH_4 and CO_2 are regarded as ideal gases; 4) Water only migrates in the fractures; 5) The adsorption and desorption of CH_4 and CO_2 in coal mass are carried out under constant temperature conditions.

2.2 Permeability Evolution Model

Assume that the coal seam is a dual-porosity unidirectional permeable medium composed of a matrix, as shown in **Figure 1**. Matrix pores are the main storage space for CH_4 and CO_2, and the change of fractures affects the evolution of permeability. Therefore, the changes of pores and fractures are the key factors in the process of CO_2 down whole injection enhanced CH_4 drainage by effects of flooding and displacement.Where a_0 is the initial matrix width, m; q is the initial fracture width, m.

The coal matrix porosity model can be expressed as (Fan et al., 2016):

$$\varphi_m = \frac{(1+S_0)\varphi_{m0} + \alpha_m (S - S_0)}{(1+S)} \tag{1}$$

where $S = \varepsilon_v + p_{mg}/(K_s + \varepsilon_a)$ is the matrix porosity strain variable; ε_v is the volume strain in the coal; p_{mg} is the gas mixture pressure, MPa; $K_s = E_s/3(1-2\nu)$ is the skeleton bulk modulus, GPa; ε_a is the skeleton adsorption gas strain; E_s is the skeleton elastic modulus, GPa; ν is Poisson ratio; $\alpha_m = 1 - K/K_s$ is the Biot coefficient for the porosity; $K = D/3(1-2\nu)$ is the bulk modulus, GPa; $D = 1/[(1/E) + 1/(a_0 \cdot K_n)]$ is the effective elastic modulus, GPa; E is the elastic modulus, GPa; K_n is fracture

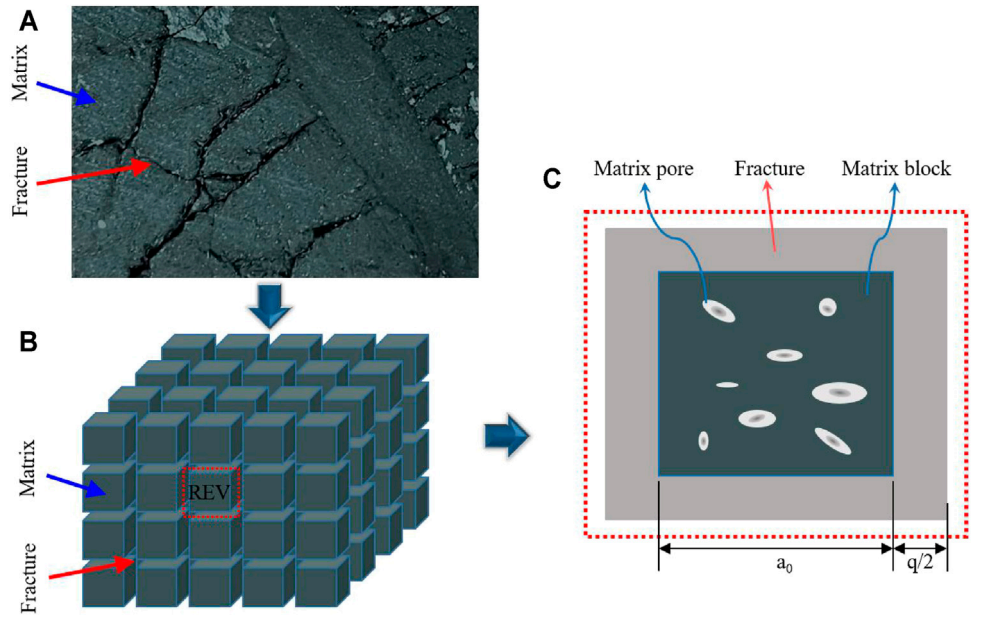

FIGURE 1 | Physical model of coal mass: **(A)** actual coal surface, **(B)** coal structure model, and **(C)** representative element volume (REV).

stiffness, GPa; and the subscript "0" represents the initial value of the parameter.

Expression of matrix swelling strain caused by gas adsorbed on coal (Cao et al., 2019):

$$\varepsilon_a = \frac{\rho_c RT \sum_{i=1}^{2} a_i \ln\left(1 + b_i p_{mgi}\right)}{E_s V_m} \tag{2}$$

where ρ_c is the density of coal, kg/m^3; R is gas molar constant, J/(mol·K); T is the temperature in the coal seam, K; a_i is the limit adsorption capacity of gas component i, m^3/kg; b_i is the adsorption equilibrium constant of gas component i, MPa^{-1}; p_{mgi} is pressure of gas component i in the matrix, Pa; V_m is the molar volume of gas, L/mol.

Considering the influence of stress and seepage effects, the fracture porosity model can be obtained as (Fan et al., 2019b):

$$\varphi_f = \varphi_{f0} - \frac{3\varphi_{f0}}{\varphi_{f0} + 3K_f/K}\left[\left(\varepsilon_a - \varepsilon_{a0}\right) - \left(\varepsilon_v - \varepsilon_{vo}\right)\right] \tag{3}$$

where φ_{f0} is the initial fracture porosity; $K_f = qK_n$ is the equivalent fracture stiffness, GPa; q is the initial fracture width, m.

According to the cubic law, the relationship between porosity and permeability is:

$$\frac{k}{k_0} = \left(\frac{\varphi_f}{\varphi_{f0}}\right)^3 \tag{4}$$

where k_0 is the initial permeability of the coal seam, m^2.

Substituting **Eq. 3** into **Eq. 4** can obtain the dynamic evolution equation of permeability:

$$\begin{aligned} k &= k_0 \cdot \left(\frac{\varphi_f}{\varphi_{f0}}\right)^3 \\ &= k_0\left\{1 - \frac{3}{\varphi_{f0} + \left(3K_f/K\right)}\left[\left(\varepsilon_a - \varepsilon_{a0}\right) - \left(\varepsilon_v - \varepsilon_{vo}\right)\right]\right\}^3 \end{aligned} \tag{5}$$

The relative permeability model of gas-water two-phase flow is (Xu et al., 2014):

$$\begin{cases} k_{rg} = k_{rg0}\left[1 - \left(\dfrac{s_w - s_{wr}}{1 - s_{wr} - s_{gr}}\right)\right]^2\left[1 - \left(\dfrac{s_w - s_{wr}}{1 - s_{wr}}\right)^2\right] \\ k_{rw} = k_{rw0}\left(\dfrac{s_w - s_{wr}}{1 - s_{wr}}\right)^4 \end{cases} \tag{6}$$

where k_{rg0} is the endpoint relative permeability of the gas; s_w is the saturation of water; s_{wr} is the irreducible water saturation; s_{gr} is the residual gas saturation fraction; k_{rw0} is the endpoint relative permeability of water.

2.3 Controlling Equation of Seepage Field

2.3.1 Gas Transport in the Coal Matrix

According to the ideal gas state equation, the density of each component gas under standard conditions is:

$$\rho_{gi} = \frac{M_{gi}}{RT} p_a \tag{7}$$

where p_a is standard atmospheric pressure, kPa.

Generalized Langmuir equation for binary gas adsorption equilibrium:

$$c_{pi} = \rho_c \rho_{gi} \frac{a_i b_i p_{mgi}}{1 + \sum_{i=1}^{2} b_i p_{mgi}} \tag{8}$$

where c_{pi} is the content of gas component i in coal, kg/m^3; ρ_{gi} is the density of gas component i under standard conditions, kg/m^3; M_{gi} is the molar mass of gas component i, g/mol.

The gas content in the coal matrix per unit volume equals the sum of the free gas content and the adsorbed gas content, which is obtained from the Langmuir equation and the ideal gas equation of state:

$$m_{mgi} = \varphi_m \rho_{gi} + c_{pi} \tag{9}$$

Owing to the influence of gas injection and drainage, the original equilibrium state of gas in the coal seam is broken. Forced by the concentration gradient, the gas in the coal matrix migrates into the fractures by diffusion. According to Fick's law of diffusion, the gas mass in the matrix can be conserved. The equation is (Ren et al., 2017):

$$\frac{\partial m_{mgi}}{\partial t} = -\frac{M_{gi}}{\tau_i RT}\left(p_{mgi} - p_{fgi}\right) \tag{10}$$

where p_{fgi} is the pressure of gas component i in the fracture, MPa; τ_i is the desorption time of gas component i, d.

Substituting **Eqs 7–9** into **Eq. 10**, the gas transport equation in the matrix can be obtained as:

$$\frac{\partial}{\partial t}\left(\varphi_m \frac{M_{gi}}{RT} p_{mgi} + \frac{M_{gi}}{RT} \frac{a_i b_i p_{mgi}}{1 + \sum_{i=1}^{2} b_i p_{mgi}} \rho_c p_a\right) = -\frac{1}{\tau_i} \frac{M_{gi}}{RT}\left(p_{mgi} - p_{fgi}\right) \tag{11}$$

2.3.2 Transport of Gas and Water in the Fractures

Considering the gas slippage effect and the generalized Darcy law of gas-water two-phase flow, the transport flows of gas and water are gained respectively (Fan et al., 2019c):

$$\begin{cases} q_{gi} = -\dfrac{k k_{rg}}{\mu_{gi}}\left(1 + \dfrac{b}{p_{fgi}}\right)\nabla p_{fgi} \\ q_w = -\dfrac{k k_{rw}}{\mu_w}\nabla p_{fw} \end{cases} \tag{12}$$

where b is the Klinkenberg factor, MPa; μ_{gi} is the dynamic viscosity of gas component i, MPa·s; μ_w is the dynamic viscosity of water, MPa·s.

Then, the mass conservation equation for gas migration in the fractures is:

$$\frac{\partial}{\partial t}\left(s_g \varphi_f \frac{M_{gi}}{RT} p_{fgi}\right) - \nabla \cdot \left(\frac{M g_i}{RT} \frac{k k_{rg}\left(p_{fgi} + b\right)}{\mu_{gi}} \nabla p_{fgi}\right) = \left(1 - \varphi_f\right) \frac{M g_i}{\tau_i RT}\left(p_{mgi} - p_{fgi}\right) \tag{13}$$

where s_g is the gas saturation in fracture, $s_g + s_w = 1$.

The water seepage controlling equation is:

$$\frac{\partial\left(s_w \varphi_f \rho_w\right)}{\partial t} - \nabla \cdot \left(\frac{\rho_w k k_{rw}}{\mu_w} \nabla p_{fw}\right) = 0 \tag{14}$$

2.4 Stress Field Controlling Equation

Considering that the total strain of coal mass is the sum of strain caused by stress, fluid pressure in matrix pores and fractures, and coal matrix swelling resulted from CH_4 and CO_2 adsorption. The stress field controlling equation is (Li et al., 2016):

$$G u_{i,jj} + \frac{G}{1 - 2v} u_{j,ji} - \left(\alpha_m p_{m,i} + \alpha_f p_{f,i}\right) - K \varepsilon_{a,i} + F_i = 0 \tag{15}$$

where $G = D/2(1 + v)$ is the shear modulus of coal, GPa; $e_{i,ij}$ are in tensor form (e can be displacement u, pressure p, or strain ε). The first subscript represents the i-direction component of variable e. The second subscript represents the partial derivative of e_i in the i-direction. The third subscript represents the partial derivative of $e_{i,ij}$ in the j direction; $a_f = 1 - K/(a_0 \cdot K_n)$ is the Biot coefficient; F_i is the volume force, GPa; $p f = s_w \cdot p_{fw} + s_g \cdot p_{fg}$ is the fracture fluid pressure, Pa.

3 SIMULATIONS OF CO_2 INJECTION ENHANCED CH_4 DRAINAGE FROM COAL SEAM

3.1 Physical Model and Definite Solution Conditions

Taking the 2,606 roadway of Zhangcun Coal Mine in Shanxi Provence as the background, the feasibility of CO_2 injection to increase gas drainage was studied in terms of its high gas and enrich water combined condition. COMSOL Multiphysics software is adopted to numerically solve the established fluid-solid coupling mathematical model. The 2,606 roadway is buried in a depth of 537 m, the coal seam temperature is 298.15 K, and the gas content during advancing is 8.5–10.0 m^3/t. As shown in **Figure 2**, a two-dimensional physical geometry model with 6 m × 16 m in size was built for the simplification of coal wall on 2,606 roadway. There are five boreholes (two for gas injection and three for drainage) arranged along the center line of the roadway with borehole spacing of 2.5 m. Line A-B is set as the observation reference of simulate results, as well as the point C (9.25 m, 3 m), point D (11.75 m, 3 m), point E (14.5 m, 3 m). Both the sides of the model are set as roller boundary condition. The overburden loading of 14.85 MPa is applied on the upper side. The extern sides of the model are set as impermeable boundaries, indicating that no gas flows at these boundaries. The bottom side is set as a fix boundary. The borehole wall of the borehole is set as the pressure boundary condition with a pumping pressure of 20 kPa and an injection pressure of 1.0 MPa. The other used parameters are shown in **Table 1**. These parameters are mainly recovered from field tests and laboratory experiments, as well as recorded

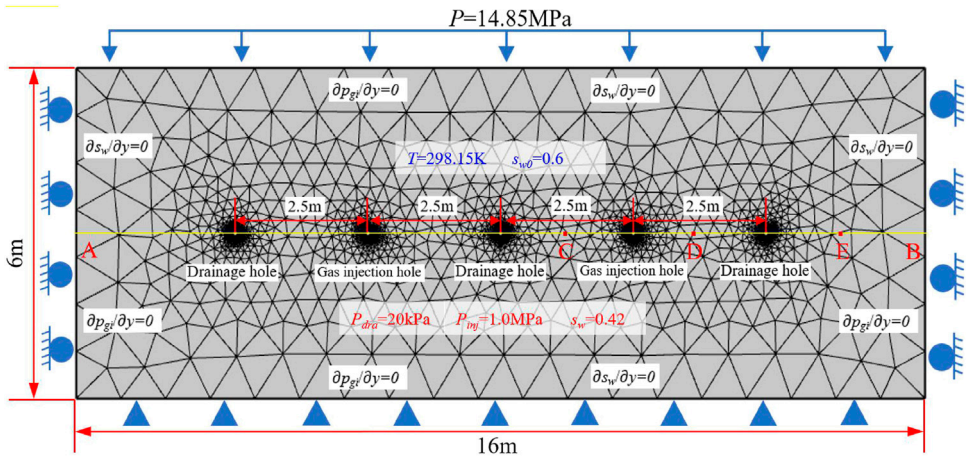

FIGURE 2 | Physical geometry model of numerical simulation.

TABLE 1 | Numerical simulation parameters.

Parameter	Value	Remark	Parameter	Value	Remark
Initial CH_4 pressure (p_0, MPa)	0.80	Field data	Initial temperature in coal seam (T, K)	298.15	Field data
Young's modulus of coal seam (E, MPa)	3,500	Experiments	Gas mole constant (R, J·mol^{-1}·K^{-1})	8.314	Fang et al. (2019b)
Young's modulus of skeleton (E_s, MPa)	8,469	Fan et al. (2019a)	Matrix initial porosity (φ_{m0})	0.04	Experiments
Poisson's ratio of coal (v)	0.30	Experiments	Initial porosity of fracture (φ_{f0})	0.018	Experiments
Langmuir constant of CH_4 (a_1, m^3 kg^{-1})	0.0323	Experiments	Initial permeability (k_0, m^2)	2.56 × 10^{-17}	Experiments
Langmuir constant of CH_4 (b_1, MPa^{-1})	0.48	Experiments	Adsorption time of CH_4 (τ_1, d)	4.34	Fan et al. (2019b)
Langmuir constant of CO_2 (a_2, m^3 kg^{-1})	0.0517	Experiments	Adsorption time of CO_2 (τ_2, d)	4.34	Fan et al. (2019b)
Langmuir constant of CO_2 (b_2, MPa^{-1})	0.7246	Experiments	Initial water saturation (s_{w0})	0.6	Fan et al. (2019a)
Dynamic viscosity of CH_4 (μ_{g1}, 10^{-5}pa s)	1.03	Fan et al. (2019a)	Irreducible water saturation (s_{wr})	0.42	Fan et al. (2019a)
Dynamic viscosity of CO_2 (μ_{g2}, 10^{-5}pa s)	1.38	Fan et al. (2019a)	Residual gas saturation (s_{gr})	0.15	Fan et al. (2019b)
Dynamic viscosity of water (μ_w, 10^{-3}pa s)	1.01	Fan et al. (2019a)	Endpoint relative permeability of water (k_{rw0})	1.0	Fan et al. (2019a)
Coal density (ρ_c, kg m^{-3})	1,380	Fang et al. (2019c)	Endpoint relative permeability of gas (k_{rg0})	0.756	Fan et al. (2016)
Klinkenberg factor (b/MPa)	0.62	Experiments			

in other articles (Fan et al., 2016; Fan et al., 2019a; Fan et al., 2019b; Fang et al., 2019b; Fang et al., 2019c).

3.2 Analysis of Simulated Results

3.2.1 Gas Pressure Evolution

Figure 3 shows the contour map of coal bed gas pressure at 10, 60, 120, and 180 days of regular gas drainage and CO_2 enhanced gas drainage. In **Figure 3A**, without CO_2 injection, the gas pressure continues to decrease with the increase of extraction time. The vertical direction decreases faster than the horizontal direction leading by the supplemental gas sources in the horizontal direction. The vertical direction is closer to the coal seam boundary and there is no supplementary gas source.

As CO_2 is continuously injected into coal seam, the gas pressure shows a downward tendency in whole, but the changes near the drainage borehole and the gas injection borehole are different, as illustrated in **Figure 3B**. The pressure around the gas injection borehole is also gradually decreasing. The pressure around the gas injection borehole drops slower than that near the extraction borehole. And the drop rate in the vertical direction is slower than that in the horizontal direction. This is because the vicinity of the injection borehole is largely affected by CO_2 flows. Although the CH_4 pressure decreases with the effects of extraction, the CO_2 pressure is rising, resulting in slowly drops of pressure. The gas pressure in the vertical direction of injection borehole is less affected by the pumping pressure of the drainage.

3.2.2 CH_4 Content Evolution

Figure 4 presents the contour of CH_4 content at 10, 60, 120, and 180 days of both regular and CO_2 enhanced gas drainage in coal seam. **Figure 4A** shows the variation of CH_4 content after regular gas drainage. The CH_4 content reduction area expands from the center of drainage borehole, but the reduction region and rate are relatively slow. On the contrary, the reduction region and rate of CH_4 content at the same duration for CO_2 injection enhanced CH_4 drainage have been significantly improved. This is caused by the combined action of CO_2 injection and CH_4 drainage. The potential pressure gradient in the coal seam drives the seepage of CO_2 and displacement of free CH_4 in the fractures. When most of the free CH_4 in the fractures is driven out, the injected CO_2 will compete with the CH_4 adsorbed inside and on the surface of the

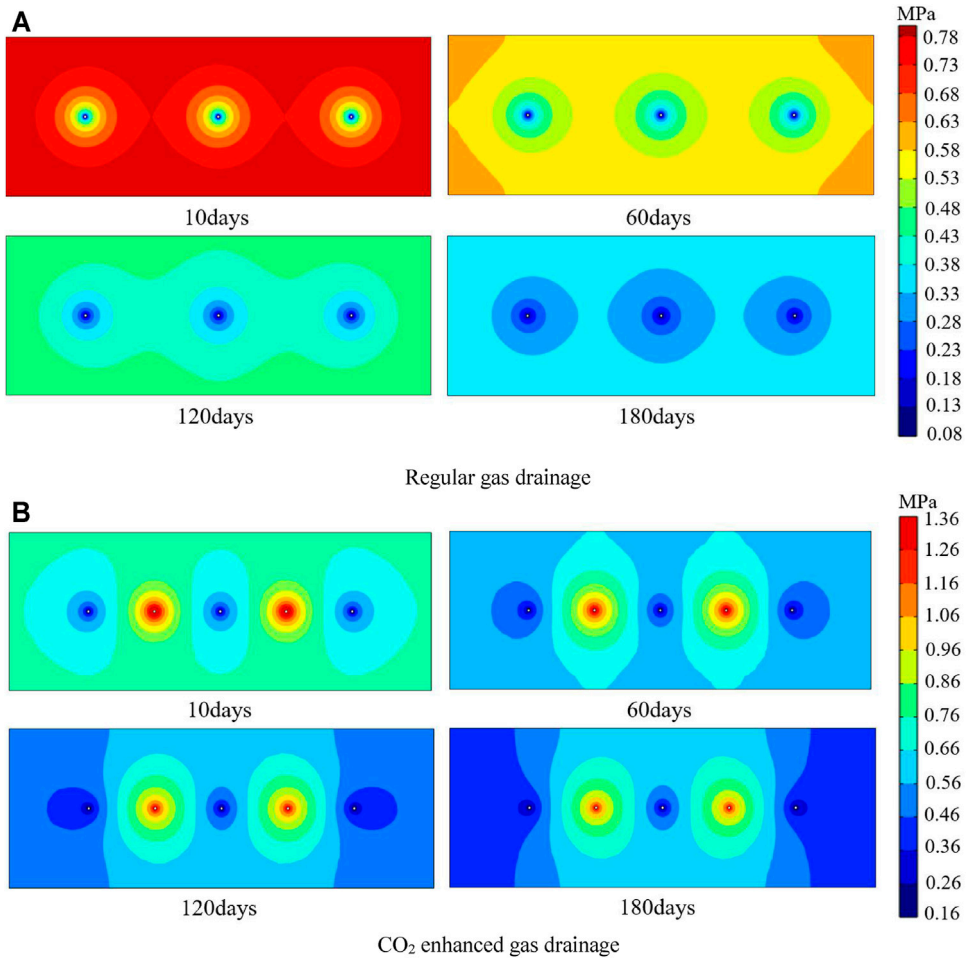

FIGURE 3 | Coal bed gas pressure distribution of both regular and CO_2 enhanced gas drainage at different times. **(A)** Regular gas drainage. **(B)** CO_2 enhanced gas drainage.

coal, and then replace the adsorbed CH_4. This accelerates the desorption rate of CH_4. In **Figure 4B**, CH_4 presents the trend of change.

Figure 5 presents the evolution of the CH_4 content on the observation line A-B with time. In **Figure 5A** CH_4 content of both regular gas drainage and CO_2 enhanced gas drainage gradually decreases with time, and the decreasing rate is highest between 10 and 60 days. CH_4 pressure in coal seam gradually decreases (pressure gradient between the drainage borehole and coal seam) as the extraction time prolongs. In other words, the pressure gradient and the CH_4 flow rate gradually decrease, slowing down the decreasing rate of CH_4 content. Compared with the regular gas drainage, the effect of CO_2 enhanced gas drainage in coal seam is more obvious with greater amount of CH_4 extracted out. The reason is that CO_2 drives and competitively adsorbs with CH_4, which enhances the efficiency CH_4 drainage.

The peak CH_4 content between the extraction borehole and the gas injection borehole for 10, 60, 120, and 180 days of regular gas drainage are 8.62, 6.87, 5.55, and 4.57 m^3/t, respectively. The peak CH_4 content of CO_2 enhanced gas drainage are 8.17, 5.69, 4.24, and 3.35 m^3/t respectively, which reduced by 5.2, 17.2, 23.6, and 26.7% compared with that of regular gas drainage, respectively. The drainage efficiency has been significantly improved.

3.2.3 Evolution of Coal Skeleton Strain and Permeability

Figure 6 shows the strain and permeability of coal skeleton adsorbed gas during regular gas drainage and CO_2 enhanced gas drainage. From **Figure 6A**, the strain value of coal skeleton behaves a gradual downward trend on the reference points (C, D, E) for the regular gas drainage. This is because the free CH_4 in fractures flows out driven by the pressure gradient, and the decrease of gas pressure in fractures triggers desorption of adsorbed gas in coals, as a result that coal matrix will shrink and deform. The strain at point E is slightly smaller than that at other points at the same time due to the influence of a single drainage hole. There is a short period of plateau on the coal permeability curve at the beginning followed by gradual increase. The change in permeability is mainly affected by effective stress and matrix shrinkage. On the one hand, with the pumping pressure of drainage, the free CH_4 in fractures is

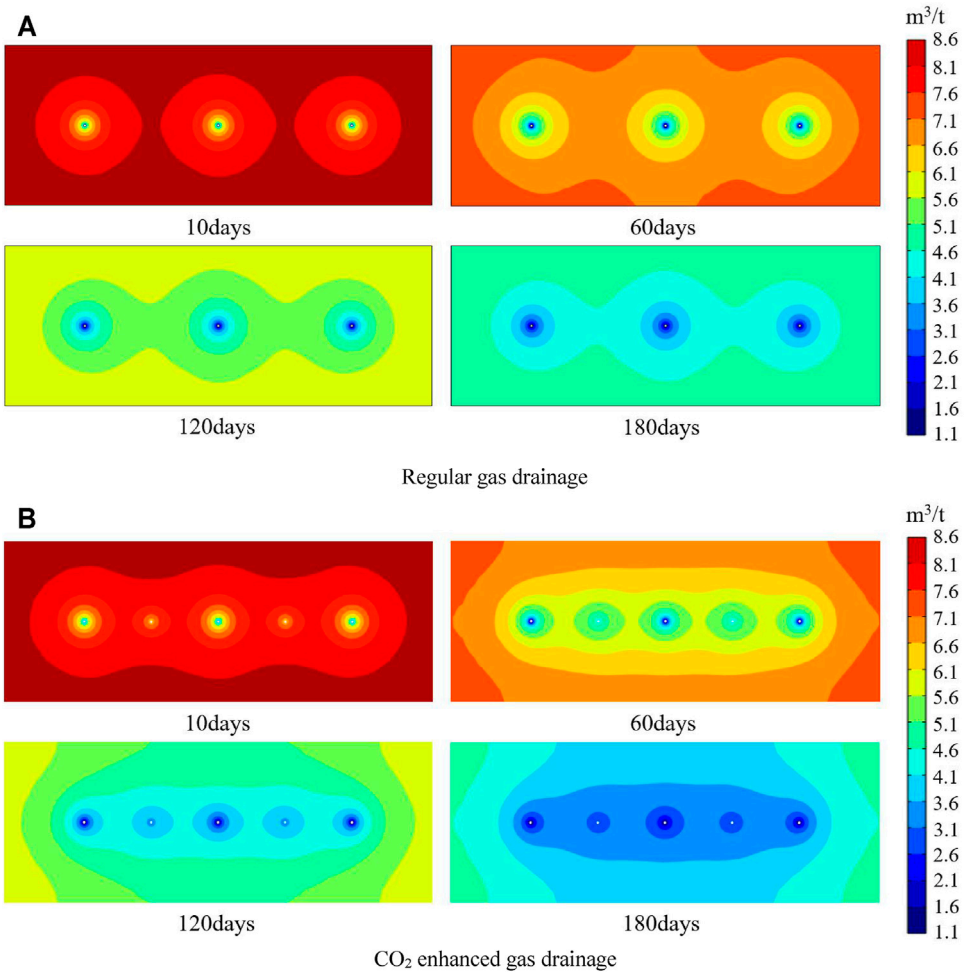

FIGURE 4 | Contour of CH_4 content of both regular and CO_2 enhanced gas drainage at different times. **(A)** Regular gas drainage. **(B)** CO_2 enhanced gas drainage.

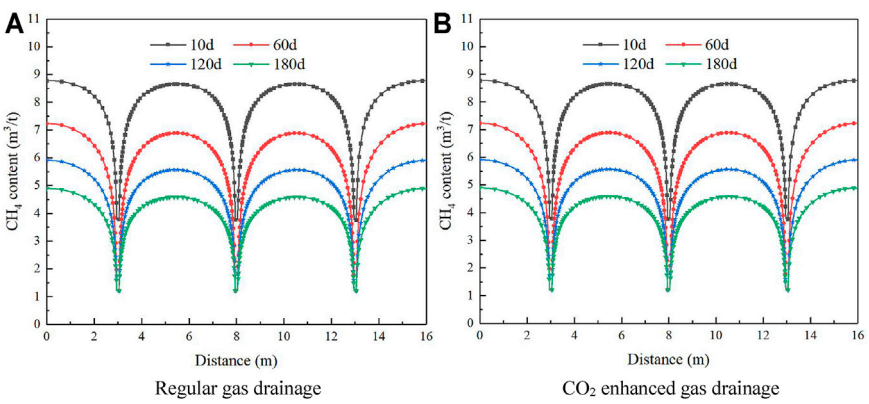

FIGURE 5 | Evolution of CH_4 content on the reference line AB with both regular and CO_2 enhanced gas drainage. **(A)** Regular gas drainage. **(B)** CO_2 enhanced gas drainage.

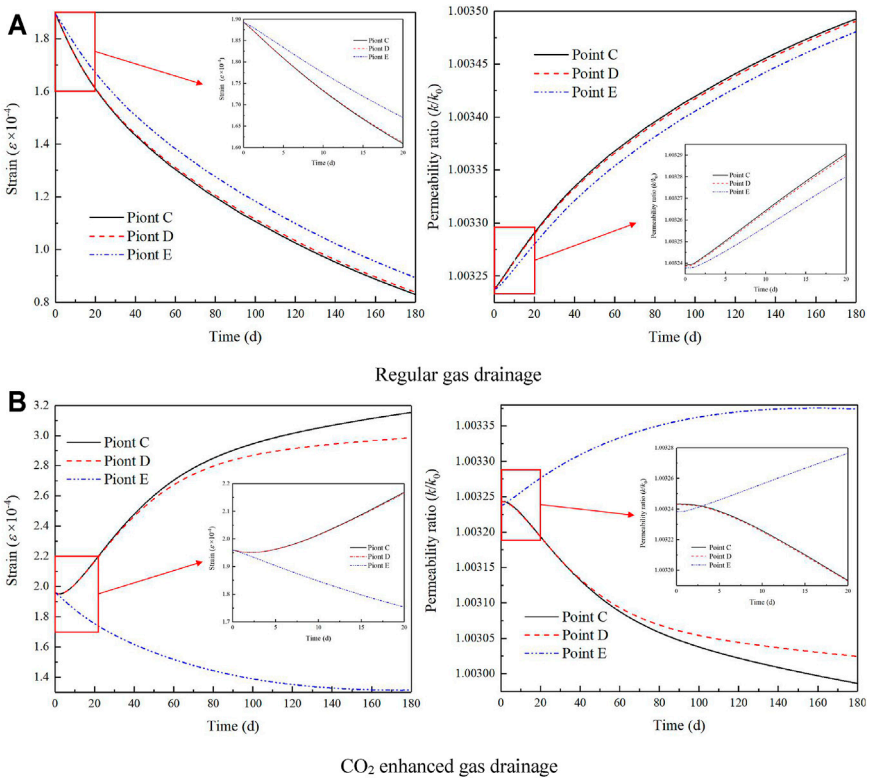

FIGURE 6 | Changes in strain and permeability of coal skeleton on the reference points (C, D, E) during regular and CO_2 enhanced gas drainage. **(A)** Regular gas drainage. **(B)** CO_2 enhanced gas drainage.

TABLE 2 | Simulation schemes of different influencing factors.

Parameter	Basic value	Variation
Injection pressure (p_{inj}, MPa)	1.0	0.6, 0.8, 1.0, 1.2
Drainage pressure (p_{dra}, kPa)	20	16, 18, 20, 22
Initial water saturation (s_{w0})	0.6	0.5, 0.6, 0.7, 0.8
Initial temperatures (T, K)	298.15	278.15, 288.15, 298.15, 308.15

discharged, and the adsorbed CH_4 begins to desorb. As a result, CH_4 pressure in coal seam drops. The effective stress increases, to compress the seepage channel in coal mass, and subsequently coal permeability decreases. On the other hand, the permeability increases caused by the CH_4 desorption induced shrinkage of coal matrix. The two opposite aspects work together to decide the change of coal seam permeability. In early stage, the seepage effect dominates, and the desorption rate of CH_4 is slow, leading to the infinitesimal change in coal permeability. When the free CH_4 is gradually discharged, the desorption rate begins to increase, and the permeability begins to rise.

In **Figure 6B**, the strain on reference points C and D shows a slight decrease—rapid increase—slow increase trend in the process of CO_2 enhanced gas drainage. CH_4 desorption under the combined action of CO_2 displacement and pumping pressure of drainage at the initial stage plays a leading role. Then, free CH_4 in the coal fractures decreases and CO_2 increases. CO_2 competes with the CH_4 in matrix for adsorption, and the strain value of coal skeleton increases as the coal matrix undergoes swelling deformation caused by the stronger adsorption affinity of CO_2 than that of CH_4. Finally, CO_2 gradually reaches adsorption equilibrium, and the strain curve gradually slows down. Point E is mainly affected by the drainage hole, and its strain value continues to decrease. **Figure 6B** shows that the evolution curve of permeability is opposite to that of coal skeleton strain.

The CH_4 desorption in coal matrix contracts leading to the decrease of coal skeleton strain. Then, as the free CH_4 in the coal fractures decreases, CO_2 increases and CO_2 competes with the CH_4 in the matrix to adsorb. The coal matrix expands and deforms, and the strain value of the coal skeleton rapidly increases. Finally, the competitive adsorption of CO_2 gradually tends to balance since most of the adsorbed CH_4 in the matrix is replaced. The competitive adsorption of CO_2 gradually tends to balance. The CO_2 adsorption rate slows down, and the strain value of coal skeleton slowly increases.

4 INFLUENCE OF DIFFERENT FACTORS ON THE DEFORMATION OF COAL SKELETON

We will explore different factors affecting the deformation of coal skeleton during CO_2 injection to enhanced CH_4 drainage from coal seam. The controlled single variable method was used to

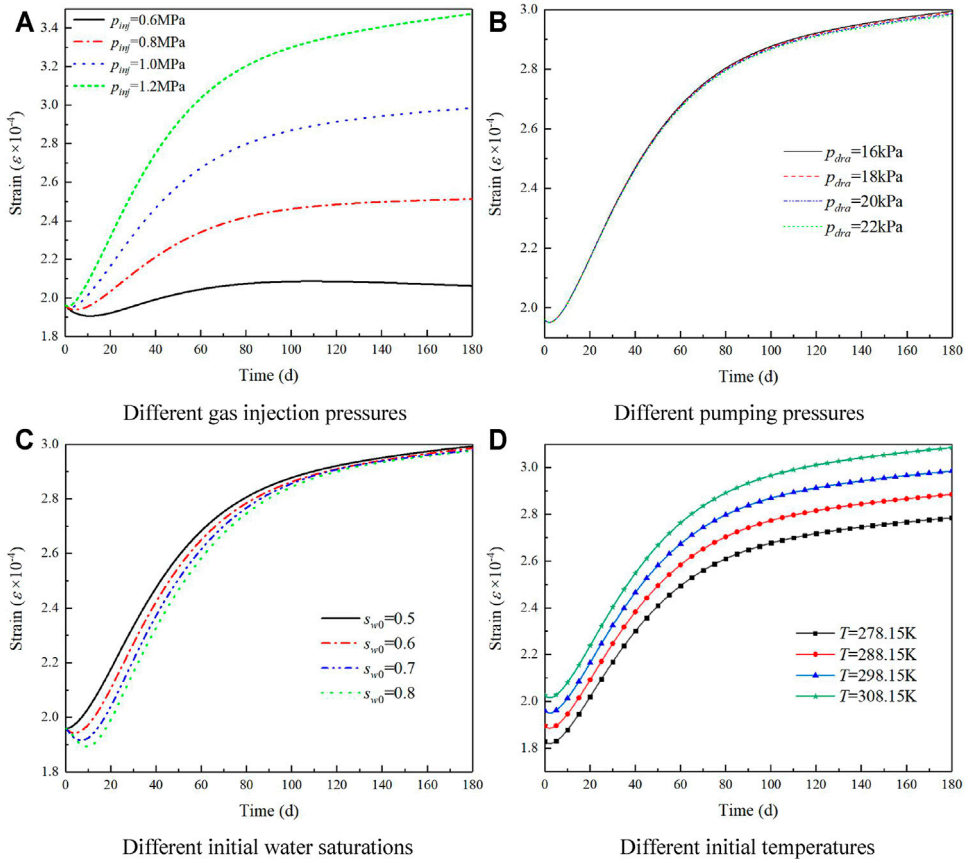

FIGURE 7 | Evolution of coal skeleton strain on point D under different parameters during CO_2 enhanced gas drainage. **(A)** Different gas injection pressures. **(B)** Different pumping pressures. **(C)** Different initial water saturations. **(D)** Different initial temperatures.

analyze the influence of different gas injection pressures, pumping pressures, initial water saturations, and coal seam temperatures on coal skeleton deformation. The simulation schemes of different influencing factors are shown in **Table 2**.

Figure 7A presents the strain curve on the reference point D under different gas injection pressures during CO_2 enhanced gas drainage. In general, higher gas injection pressure will lead to greater strain of coal skeleton. Higher injection pressure under the same condition will lead to greater amount of adsorbed CO_2, as well as greater swelling deformation of coal matrix. If the injection pressure is low, the matrix contraction in the early stage is great, and the curve is easy to slow down. When the initial injection pressure is higher than CH_4 pressure in coal seam, CO_2 cannot transport from high pressure to low pressure area. At this time, the coal skeleton strain is mainly affected by the desorption of CH_4. CH_4 pressure in coal seam gradually decreases as the action of pumping pressure. When CH_4 pressure drops below the injection pressure, CO_2 can flow under the action of the pressure gradient. The lower the injection pressure of CO_2, the smaller the pressure gradient formed. As a result, the adsorption equilibrium reaches earlier.

In **Figure 7B**, the change of pumping pressure of drainage affects the deformation of coal skeleton slightly.

Figure 7C shows the strain curve of coal skeleton on the reference point D at different initial water saturations. Greater initial water saturation will lead to greater deformation of the coal skeleton in the early stage, and the strain value of coal skeleton gradually tends to be consistent as the operation time of gas injection prolongs. The reason is the water in fractures flow out will carry out part of the free CH_4 and CO_2 in the coal. As a result, the desorption rate of CH_4 is accelerated and the adsorption rate of CO_2 is slowed down. The shrinkage scale of the coal matrix becomes larger. As most of the water flows out of the borehole, the water saturation of coal seams with different water saturations tends to be consistent, and the deformation of coal skeleton also tends to be consistent.

Figure 7D shows the coal skeleton strain on the reference point D at different initial temperatures. The higher initial temperature will lead to greater reduction in the coal skeleton strain value, particularly when the operation time of gas injection prolongs.

5 CONCLUSION

1) A fluid-solid coupling mathematical model of CO_2 injection enhanced CH_4 drainage in coal seam was

established based on Fick's law, Darcy's law, ideal gas state equation, and Langmuir equation. Meanwhile, numerical simulations on CO_2 injection enhanced CH_4 drainage during underground mining were carried out using the established model.

2) The CH_4 content of both regular and CO_2 enhanced gas drainage gradually decreases with time, and the decreasing rate is high between 10 and 60 days. Compared with regular gas drainage, CO_2 enhanced gas drainage effect is more obvious with greater amount of CH_4 extracted out. When the CH_4 in coal seam is extracted for 10, 60, 120, and 180 days, the CH_4 content in coal seam is reduced by 5.2, 17.2, 23.6, and 26.7%, respectively.
3) For regular gas drainage, the deformation of the coal skeleton is dominated by the contraction of coal matrix induced by gas desorption, and the strain curve shows a continuous downward trend. In the process of CO_2 enhanced gas drainage, the strain curve of coal skeleton showed a slight decrease— rapid increase—slow increase trend. The evolution curve of permeability is opposite to that of coal skeleton strain.
4) Higher gas injection pressure will lead to greater coal skeleton strain. The pumping pressure affects the deformation of coal skeleton slightly compared with the initial water saturation and initial temperature. Greater initial water saturation will lead to larger deformation of coal skeleton in the early stage, and the strain value of coal skeleton gradually tends to be consistent as the operation time of gas injection prolongs. Higher initial temperature leads to greater reduction in coal skeleton strain, particularly when the gas injection prolongs continuously.

DATA AVAILABILITY STATEMENT

The raw data supporting the conclusion of this article will be made available by the authors, without undue reservation.

AUTHOR CONTRIBUTIONS

CF write and financially support this paper; LY design the research scheme and write this paper; GW financially support and correct this paper; QH derive the equations of this paper; HW carry out simulations.

FUNDING

This research was financially supported by the National Natural Science Foundation of China (Grant Nos. 52174117, 52004117, and 51874159), the Research Fund of Key Laboratory of Mining Disaster Prevention and Control (Grant No. MDPC202008), the Basic Research Project of Key Laboratory of Liaoning Provincial Education Department (Grant No. LJ2020JCL005), and the Project supported by the Postdoctoral Science Foundation of China (Grant Nos. 2021T140290, 2020M680975), the Project supported by discipline innovation team of Liaoning Technical University (Grant no. LNTU20TD-30).

ACKNOWLEDGMENTS

The author(s) would like to thank all editors and reviewers for their comments and suggestions.

REFERENCES

Baran, P., Zarębska, K., Krzystolik, P., Hadro, J., and Nunn, A. (2014). CO_2-ECBM and CO_2 Sequestration in Polish Coal Seam - Experimental Study. *J. Sustainable Min.* 13 (2), 22–29. doi:10.7424/jsm140204

Busch, A., Krooss, B. M., Gensterblum, Y., van Bergen, F., and Pagnier, H. J. M. (2003). High-Pressure Adsorption of Methane, Carbon Dioxideand Their Mixtures on Coals with a Special Focus on the Preferential Sorption Behaviour. *J. Geochem. Explor.* 78-79, 671–674. doi:10.1016/s0375-6742(03)00122-5

Cao, Z., Lin, B., and Liu, T. (2019). The Impact of Depositional Environment and Tectonic Evolution on Coalbed Methane Occurrence in West Henan, China. *Int. J. Min. Sci. Technol.* 29 (2), 297–305. doi:10.1016/j.ijmst.2019.01.006

Chattaraj, S., Mohanty, D., Kumar, T., and Halder, G. (2016). Thermodynamics, Kinetics and Modeling of Sorption Behaviour of Coalbed Methane - A Review. *J. Unconv. Oil Gas Resour.* 16, 14–33. doi:10.1016/j.juogr.2016.09.001

Fan, C. J., Li, S., Luo, M. K., Yang, Z. H., Zhang, H. H., and Wang, S. (2016). Numerical Simulation of Deep Coalbed Methane Extraction Based on Fluid-Solid-thermal Coupling. *J. China Coal Society* 41 (12), 3076–3085. (in Chinese with English abstract).

Fan, C., Li, S., Luo, M., Du, W., and Yang, Z. (2017). Coal and Gas Outburst Dynamic System. *Int. J. Min. Sci. Technol.* 27 (01), 49–55. doi:10.1016/j.ijmst.2016.11.003

Fan, Y., Deng, C., Zhang, X., Li, F., Wang, X., and Qiao, L. (2018). Numerical Study of CO2-enhanced Coalbed Methane Recovery. *Int. J. Greenhouse Gas Control.* 76, 12–23. doi:10.1016/j.ijggc.2018.06.016

Fan, C., Elsworth, D., Li, S., Zhou, L., Yang, Z., and Song, Y. (2019). Thermo-hydro-mechanical-chemical Couplings Controlling CH_4 Production and CO_2 Sequestration in Enhanced Coalbed Methane Recovery. *Energy* 173, 1054–1077. doi:10.1016/j.energy.2019.02.126

Fan, C., Elsworth, D., Li, S., Chen, Z., Luo, M., Song, Y., et al. (2019). Modelling and Optimization of Enhanced Coalbed Methane Recovery Using CO_2/N_2 Mixtures. *Fuel* 253, 1114–1129. doi:10.1016/j.fuel.2019.04.158

Fan, C., Li, S., Luo, M., Yang, Z., and Lan, T. (2019). Numerical Simulation of Hydraulic Fracturing in Coal Seam for Enhancing Underground Gas Drainage. *Energy Explor. Exploit.* 37 (1), 166–193. doi:10.1177/0144598718785998

Fang, H. H., Sang, S. X., and Liu, S. Q. (2019). The Coupling Mechanism of the thermal-hydraulic- Mechanical fields in CH_4-Bearing Coal and its Application in the CO_2-enhanced Coalbed Methane Recovery. *J. Petrol. Sci. Eng.* 181, 106177. doi:10.1016/j.petrol.2019.06.041

Fang, H., Sang, S., and Liu, S. (2019). Establishment of Dynamic Permeability Model of Coal Reservoir and its Numerical Simulation during the CO_2-ECBM Process. *J. Pet. Sci. Eng.* 179, 885–898. doi:10.1016/j.petrol.2019.04.095

Fang, H.-H., Sang, S.-X., and Liu, S.-Q. (2019). Numerical Simulation of Enhancing Coalbed Methane Recovery by Injecting CO_2 with Heat Injection. *Pet. Sci.* 16 (1), 32–43. doi:10.1007/s12182-018-0291-5

Guo, D., Lv, P., Zhao, J., and Zhang, C. (2020). Research Progress on Permeability Improvement Mechanisms and Technologies of Coalbed Deep-Hole Cumulative Blasting. *Int. J. Coal Sci. Technol.* 7 (2), 329–336. doi:10.1007/s40789-020-00320-5

Huo, B., Jing, X., Fan, C., and Han, Y. (2019). Numerical Investigation of Flue Gas Injection Enhanced Underground Coal Seam Gas Drainage. *Energy Sci. Eng.* 7 (6), 3204–3219. doi:10.1002/ese3.491

Li, S., Fan, C., Han, J., Luo, M., Yang, Z., and Bi, H. (2016). A Fully Coupled thermal-hydraulic-mechanical Model with Two-phase Flow for Coalbed Methane Extraction. *J. Nat. Gas Sci. Eng.* 33, 324–336. doi:10.1016/j.jngse.2016.05.032

Lin, J., Ren, T., Wang, G., Booth, P., and Nemcik, J. (2017). Experimental Study of the Adsorption-Induced Coal Matrix Swelling and its Impact on ECBM. *J. Earth Sci.* 28 (5), 917–925. doi:10.1007/s12583-017-0778-9

Lin, J., Ren, T., Wang, G., Booth, P., and Nemcik, J. (2018). Experimental Investigation of N_2 Injection to Enhance Gas Drainage in CO_2-rich Low Permeable Seam. *Fuel* 215, 665–674. doi:10.1016/j.fuel.2017.11.129

Liu, J., Yao, Y., Liu, D., and Elsworth, D. (2017). Experimental Evaluation of CO_2 Enhanced Recovery of Adsorbed-Gas from Shale. *Int. J. Coal Geol.* 179, 211–218. doi:10.1016/j.coal.2017.06.006

Liu, J., Xie, L., Elsworth, D., and Gan, Q. (2019). CO_2/CH_4 Competitive Adsorption in Shale: Implications for Enhancement in Gas Production and Reduction in Carbon Emissions. *Environ. Sci. Technol.* 53 (15), 9328–9336. doi:10.1021/acs.est.9b02432

Pan, J., Lv, M., Hou, Q., Han, Y., and Wang, K. (2019). Coal Microcrystalline Structural Changes Related to Methane Adsorption/desorption. *Fuel* 239, 13–23. doi:10.1016/j.fuel.2018.10.155

Ren, T., Wang, G., Cheng, Y., and Qi, Q. (2017). Model Development and Simulation Study of the Feasibility of Enhancing Gas Drainage Efficiency through Nitrogen Injection. *Fuel* 194, 406–422. doi:10.1016/j.fuel.2017.01.029

Reznik, A. A., Singh, P. K., and Foley, W. L. (1984). An Analysis of the Effect of CO_2 Injection on the Recovery of *In-Situ* Methane from Bituminous Coal: An Experimental Simulation. *Soc. Pet. Eng. J.* 24 (05), 521–528. doi:10.2118/10822-PA

Song, Y., Jang, B., and Lan, F. J. (2019). Competitive Adsorption of $CO_2/N_2/CH_4$ onto Coal Vitrinite Macromolecular: Effects of Electrostatic Interactions and Oxygen Functionalities. *Fuel* 235, 23–38./doi:10.1016/j.fuel.2018.07.087

Vishal, V., Singh, T. N., and Ranjith, P. G. (2015). Influence of Sorption Time in CO_2 -ECBM Process in Indian Coals Using Coupled Numerical Simulation. *Fuel* 139, 51–58. doi:10.1016/j.fuel.2014.08.009

Wang, T., Tian, S., Li, G., Sheng, M., Ren, W., Liu, Q., et al. (2018). Molecular Simulation of CO_2/CH_4 Competitive Adsorption on Shale Kerogen for CO_2 Sequestration and Enhanced Gas Recovery. *J. Phys. Chem. C* 122 (30), 17009–17018. doi:10.1021/acs.jpcc.8b02061

Wang, K., Pan, J., Wang, E., Hou, Q., Yang, Y., and Wang, X. (2020). Potential Impact of CO_2 Injection into Coal Matrix in Molecular Terms. *Chem. Eng. J.* 401, 126071. doi:10.1016/j.cej.2020.126071

Wu, S., Deng, C., and Wang, X. (2019). Molecular Simulation of Flue Gas and CH_4 Competitive Adsorption in Dry and Wet Coal. *J. Nat. Gas Sci. Eng.* 71, 102980. doi:10.1016/j.jngse.2019.102980

Xu, H., Tang, D. Z., Tang, S. H., Zhao, J. L., Meng, Y. J., and Tao, S. (2014). A Dynamic Prediction Model for Gas-Water Effective Permeability Based on Coalbed Methane Production Data. *Int. J. Coal Geology* 121, 44–52. doi:10.1016/j.coal.2013.11.008

Yi, H., Li, F., Ning, P., Tang, X., Peng, J., Li, Y., et al. (2013). Adsorption Separation of CO_2, CH_4, and N_2 on Microwave Activated Carbon. *Chem. Eng. J.* 215-216, 635–642. doi:10.1016/j.cej.2012.11.050

Zhou, L., Feng, Q., Chen, Z., and Liu, J. (2012). Modeling and Upscaling of Binary Gas Coal Interactions in CO2 Enhanced Coalbed Methane Recovery. *Proced. Environ. Sci.* 12, 926–939. doi:10.1016/j.proenv.2012.01.368

Conflict of Interest: The authors declare that the research was conducted in the absence of any commercial or financial relationships that could be construed as a potential conflict of interest.

Publisher's Note: All claims expressed in this article are solely those of the authors and do not necessarily represent those of their affiliated organizations, or those of the publisher, the editors and the reviewers. Any product that may be evaluated in this article, or claim that may be made by its manufacturer, is not guaranteed or endorsed by the publisher.